Impact of Non-Uniform Carrier Density on the Determination of Metal Induced Recombination Losses

David Herrmann[1, a)], Andreas Fell[1, 2, b)], Hannes Höffler[1, c)], Sabrina Lohmüller[1, d)], Andreas Wolf[1, e)]

[1]*Fraunhofer Institute for Solar Energy Systems ISE, Heidenhofstraße 2, 79110 Freiburg, Germany*
[2]*AF simulations, Landstr. 12, 79232 March, Germany*

[a)]Corresponding author: david.herrmann@ise.fraunhofer.de
[b)]andreas@quokka.com
[c)]hannes.hoeffler@ise.fraunhofer.de
[d)]sabrina.lohmueller@ise.fraunhofer.de
[e)]andreas.wolf@ise.fraunhofer.de

Abstract. We evaluate in detail the impact of sample properties on the accuracy of a simple *area-weighted approach* to determine the local dark saturation current density at metal contacts $j_{0,met}$. Using metallized samples, we further compare the apparent $j_{0,met}$ resulting from this simple approach to the $j_{0,met}$ value determined using numerical simulations with Quokka3. The analysis shows that the assumption of a uniform carrier density of the *area-weighted approach* leads to a significant underestimation of $j_{0,met}$ which depends strongly on sample properties as e.g. the base resistivity ρ_B and $j_{0,met}$ itself. This is confirmed by experimental data using conventional metallized samples, which demonstrate an underestimation of $j_{0,met}$ of up to 20% when using the *area-weighted approach* compared to numerical simulations.

INTRODUCTION

One dominating loss mechanism for currently relevant solar cells—e.g. passivated emitter and rear cell (PERC)—is charge carrier recombination at the metal contacts [1,2]. For the development of advanced emitters, metallization technologies as well as accurate device simulation, a precise quantification of the metal induced recombination losses in terms of the local dark saturation current density $j_{0,met}$ is essential. Most authors use an area-weighted model to quantify $j_{0,met}$ from globally measured quantities like (implied) voltage or photoluminescence signal [3–5]. Here, one critical aspect is the assumption of a uniform excess carrier density Δn and thereby *pn* product $(N_{dop} + \Delta n)\Delta n$, with N_{dop} being the dopant concentration. This assumption leads to a strong underestimation of the determined $j_{0,met}$ as shown in Ref. [6,7]. In this work, we perform numerical simulations using Quokka3 [8] to evaluate the influence of different sample specific properties/structures on the non-uniformity of the *pn* product and thus the deviation of the apparent dark saturation current density $j_{0,met}$ that results from the evaluation using an *area-weighted approach*. This enables the choice of suitable sample properties for minimizing the impact of the non-uniformity of the *pn* product as well as the rough correction of literature data that was generated using the *area-weighted approach*.

Finally, for metallized samples we determine the dark saturation current density $j_{0,met}$ using a *simulative approach*, which accounts for the non-uniformity of the *pn* product [6,9] and compare the results to the apparent $j_{0,met}$ determined using the *area-weighted approach* for the same data.

SiliconPV 2019, the 9th International Conference on Crystalline Silicon Photovoltaics
AIP Conf. Proc. 2147, 020005-1–020005-7; https://doi.org/10.1063/1.5123810
Published by AIP Publishing. 978-0-7354-1892-9/$30.00

APPROACH

Impact of Sample Properties on the Area-Weighted Approach

The approach under investigation in this work is similar as described in Ref. [10], where a detailed description is given. The workflow of this *area-weighted approach* is as follows: Firstly, for non-metallized reference samples a quasi steady state photoconductance (QSSPC) and a photoluminescence imaging (PLI) measurement is performed to calibrate the average PLI signal $\bar{\varphi}$ in the area where the QSSPC measurement is performed, to the iV_{oc} measured by QSSPC. For the simulation, we calibrate the average simulated signal $\bar{\varphi}$ of the symmetry element to the iV_{oc} determined for this symmetry element. Applying this calibration, the PLI signal for single side metallized and non-metallized samples is associated to an iV_{oc} and further to a global dark saturation current density j_0 each, using the one-diode equation and the known photocurrent absorbed by the sample. During the measurement, the non-metallized side of the sample points towards the detector and illumination source. The *area-weighted* model approximates the global saturation current density of the sample by

$$j_0 = (1 - F) \cdot j_{0,\mathrm{pas}} + F \cdot j_{0,\mathrm{met}} + j_{0,\mathrm{bulk+front}}, \quad \textbf{(1)}$$

with the metallization area fraction F of the partly metallized rear surface, the local saturation current density in the metallized and passivated area $j_{0,\mathrm{met}}$ and $j_{0,\mathrm{pas}}$, as well as the lumped value for front surface and bulk $j_{0,\mathrm{bulk+front}}$. Thus, with the global difference $\Delta j_0 = j_{0,\mathrm{metal.}} - j_{0,\mathrm{non\text{-}metal}}$ induced by the metallization, Eq. (2) yields the apparent recombination parameter

$$j_{0,\mathrm{met}} = \Delta j_0 / F + j_{0,\mathrm{pas}}, \quad \textbf{(2)}$$

in the metallized region using the known parameters F and $j_{0,\mathrm{pas}}$.

In this work, we evaluate the influence of sample specific properties/structures on the result of the *area-weighted approach* using simulated PLI and simulated QSSPC data as input. Certain parameters in this simulations are varied in reasonable ranges, to evaluate their impact on the apparent $j_{0,\mathrm{met}}$ resulting from the *area-weighted approach*. In detail, we investigate the influence of the base resistivity ρ_B, the presence of an emitter ($n^+/n/n^+$ or $p^+/n/p^+$ structure), the finger width w and the $j_{0,\mathrm{met,sim}}$ input value to the simulation. Besides PLI and QSSPC data, other measurement data might be used as input to the one diode equation of the *area weighted approach* [4,5], e.g. suns-V_{oc}-curves [11].

Experimental Comparison Between Area-Weighted and Simulative Approach

Additionally to the *area-weighted approach*, we perform a *simulative approach*, which is based on numerical PLI simulations using Quokka3. A detailed description of this *simulative approach* is given in Ref. [6,9]. For the comparison of these two approaches, we use metallized samples with varying metallization fraction F, Figure 1 shows the schematic process flow for the sample preparation. We start with n-type Czochralski (Cz) grown Silicon wafers with an edge length of 156 mm, a thickness $W \approx 170$ µm after alkaline texture and $\rho_B \approx 4.0$ Ωcm, determined

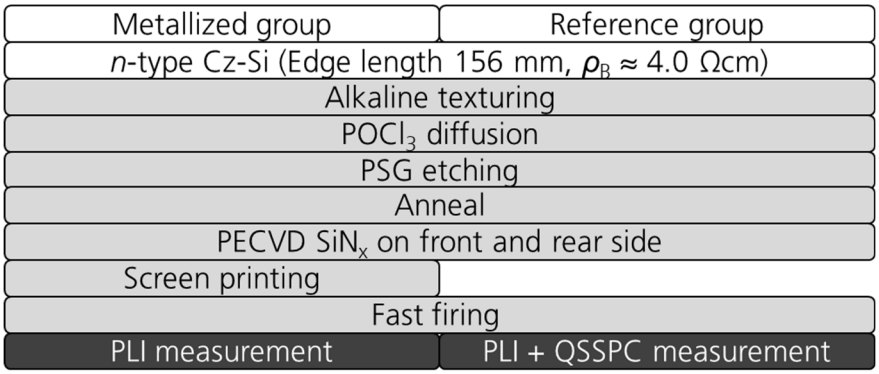

FIGURE 1: Process flow for the fabrication of $n^+/n/n^+$ samples with one-sided metallization, used for the comparison between the *area-weighted* and the *simulative approach*. Additionally, non-metallized reference samples are processed.

after thermal donor annihilation [12]. After alkaline texturing, the $POCl_3$-based diffusion process forms highly n^+-doped regions on both sides of the samples ($n^+/n/n^+$ structure) with a sheet resistance $R_{sh} \approx 105\ \Omega/\square$. Subsequently, we etch the phosphosilicate glass (PSG) layer, perform an annealing step [13] and passivate the front and rear side using plasma enhanced chemical vapor deposition (PECVD). The metallization is realized via screen printing a commercially available silver paste using full area screens with varying metallization fractions $F \approx 4\%$ and $F \approx 13.3\%$, consisting of just fingers (no busbars) with a width of $w \approx 40\ \mu m$ (screen opening width). This is followed by a firing step in a fast firing oven (FFO) with a peak set temperature of $T_{FFO} = 840\ °C$. Finally, we perform QSSPC and PLI measurements. The reference group is processed similarly but without screen printing. For the latter, we determine the dark saturation current density at the passivated surface to $j_{0,pas} \approx 55\ fA/cm^2$ using QSSPC measurements as described in Ref. [14]. PLI measurements yield the signal $\bar{\varphi}_{met}$ for each metallized sample as well as the signal $\bar{\varphi}_{ref}$ for the non-metallized reference.

For the determination of $j_{0,met}$ using the *simulative approach* [6,9], we replicate a non-metallized reference sample with all known sample properties in a Quokka3 simulation and calculate the bulk lifetime $\tau_b(\Delta n)$ to reproduce the effective carrier lifetime $\tau_{eff}(\Delta n)$ measured by QSSPC. Simulations also yield a PLI signal $\bar{\varphi}_{ref,sim}$ for the reference sample. Subsequently, we implement the geometry of the metallized samples to the simulation, using the finger width w and the finger distance d determined for the respective sample. Thereafter, we vary $j_{0,met}$ and fix it to the value at which the ratio of the simulated PLI signals $\bar{\varphi}_{met,sim}/\bar{\varphi}_{ref,sim}$ equals the ratio of the measured PLI signals $\bar{\varphi}_{met}/\bar{\varphi}_{ref}$.

RESULTS

The first part of this section describes the impact of characteristic sample properties/structures on the apparent $j_{0,met}$ that the *area-weighted approach* would yield, theoretically evaluated using numerical simulations as described above. The second part shows a comparison between the *area-weighted* and the *simulative approach* using measured data obtained from the metallized samples.

Influencing Parameters for the Area-Weighted Approach

In Ref. [6] the authors show, that for the *area-weighted approach* the assumption of a uniform *pn* product in the entire sample leads to a significant underestimation of $j_{0,met}$. Here, we evaluate the impact of certain characteristic parameters on the degree of underestimation for $j_{0,met}$. For all simulations performed in this chapter, the input parameters stated in Table 1 are fixed. The input parameters were adjusted such that they reflect realistic processes currently used for PERC solar cells. The simulations assume *n*-type bulk material, a sample thickness of $W = 170\ \mu m$ and an intrinsic (Auger + radiative recombination) bulk lifetime τ_B. The sheet resistance R_{sh} is set to $R_{sh} = 100\ \Omega/\square$, the dark saturation current density in the passivated region to $j_{0,pas} = 60\ fA/cm^2$ and the simulations were performed at room temperature $T = 298.15\ K$ with an illumination intensity of $I = 2.5e17\ Photons/cm^2s$ (corresponding to a generation current density of $j_{gen} = 39.5\ mA/cm^2$) at a wavelength of $\lambda = 790\ nm$, the reflection of the sample is set to the standard PERC reflectivity from Quokka3, which corresponds to $R_{790nm} \approx 1.3\%$ at this wavelength. Surface doping type (n^+ or p^+), base resistivity ρ_B, finger width w and the $j_{0,met,sim}$ input values are varied parameters.

TABLE 1: Fixed input parameters used for all PLI simulations, which were performed to evaluate the influence of the respective parameters on the apparent $j_{0,met}$.

Description	Value	Unit
Bulk material	*n*-type	-
Bulk lifetime τ_B	intrinsic	-
Thickness W	170	µm
Sheet resistance R_{sh}	100	Ω/□
Dark saturation current density in the passivated area $j_{0,pas}$	60	fA/cm^2
Temperature T	298.15	K
Illumination intensity I	2.5e17	$Photons/cm^2s$ (at 790 nm)
Reflectivity R	Std. PERC reflectivity curve (textured surface)	

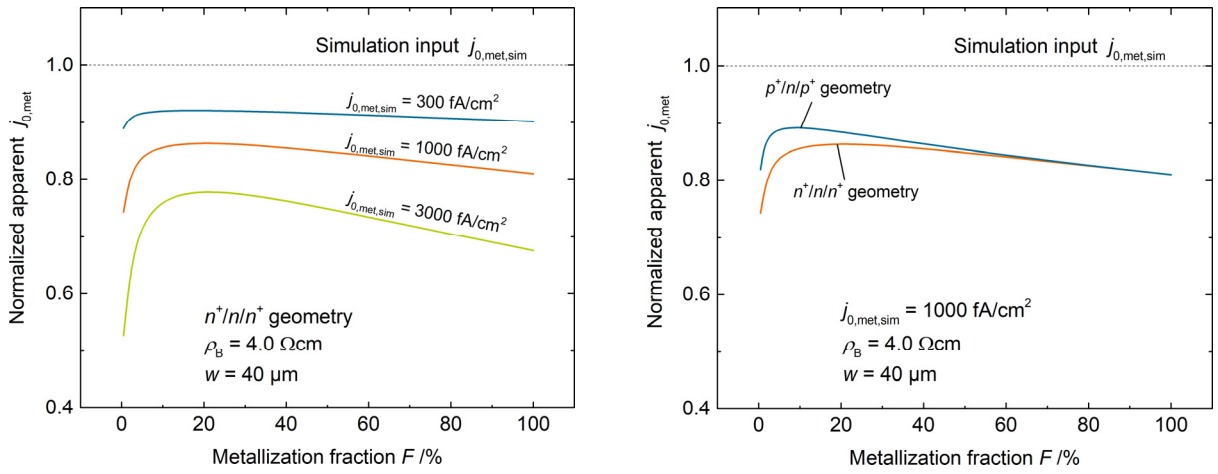

FIGURE 2: Apparent $j_{0,met}$ using the *area-weighted approach*, normalized with the input of the simulation $j_{0,met,sim}$, given as a function of the metallization fraction F. (a) shows the influence of the input $j_{0,met,sim}$ itself on the apparent $j_{0,met}$ for a $n^+/n/n^+$ structure with ρ_B = 4 Ωcm and w = 40 µm. (b) shows the influence of the presence ($p^+/n/p^+$) or absence ($n^+/n/n^+$) of an emitter on the resulting apparent $j_{0,met}$ for $j_{0,met,sim}$ = 1000 fA/cm².

Figure 2 (a) shows the impact of the simulation input $j_{0,met,sim}$ itself on the apparent $j_{0,met}$ values that would be determined using the *area-weighted approach* as a function of the metallization fraction F. The simulations are performed assuming a $n^+/n/n^+$ structure with $w = 40$ µm and $\rho_B = 4$ Ωcm. For $j_{0,met,sim} = 300$ fA/cm² the apparent $j_{0,met}$ is almost independent on F and the *area-weighted approach* underestimates $j_{0,met,sim}$ by ~10%, i.e. the ratio of apparent $j_{0,met}$ to simulation input is $j_{0,met}/j_{0,met,sim} \approx 0.9$. By increasing $j_{0,met,sim}$ to 1000 fA/cm², the underestimation becomes stronger and a dependency on F arises. For a very low metallization fraction $F \approx 0.4\%$, the degree of underestimation is strongest with $j_{0,met}/j_{0,met,sim} \approx 0.74$. When F increases to $F \approx 20\%$, the ratio increases to $j_{0,met}/j_{0,met,sim} \approx 0.86$. Increasing F further to $F = 100\%$—a one-sided fully metallized sample—the deviation is again more pronounced with $j_{0,met}/j_{0,met,sim} \approx 0.81$. Inputting $j_{0,met,sim}$= 3000 fA/cm² into the simulation, the underestimation and the dependency on F increase once more. For $F \approx 0.4\%$, the ratio of the apparent value to input value is as low as $j_{0,met}/j_{0,met,sim} \approx 0.53$. At $F \approx 20\%$ the ratio reaches a maximum of approximately 0.78 and for $F = 100\%$ it decreases again to 0.67.

The underestimation originates from a gradient of the *pn* product within the sample, where the *pn* product is smaller at the metal contacts due to enhanced local recombination. For small F values the gradient is mostly of lateral nature and for large F values it is mostly of vertical nature, explaining the course of the curve with a maximum at approximately $F \approx 20\%$. A detailed description of this effect is given in Ref. [6].

Figure 2 (b) shows the influence of the presence or absence of an emitter at the sample front and rear surface ($n^+/n/n^+$ vs. $p^+/n/p^+$ structure). The simulations are performed with $w = 40$ µm, $\rho_B = 4$ Ωcm and $j_{0,met,sim} = 1000$ fA/cm². For $F > 50\%$ the results are similar, since the gradient in the *pn* product is mostly vertical and the highly doped regions at the surface only affect the lateral charge carrier transport. For $F < 50\%$ the underestimation is stronger for the $n^+/n/n^+$ geometry and the difference between the structures increases for decreasing F. This characteristic results from the fact, that holes are minority charge carriers in the *n*-doped bulk and in the highly *n*-doped surface regions for the $n^+/n/n^+$ structure and therefore their lateral transport is less strong compared to the $p^+/n/p^+$ structure. Here, holes can propagate into the highly *p*-doped surface region (emitter), where they become majority charge carriers and their lateral transport is facilitated. Thus, for the $p^+/n/p^+$ structure, lateral balancing currents reduce the lateral gradient in the *pn* product. This results in a smaller underestimation for this structure, since the underestimation depends on the gradient of the *pn* product [6].

Figure 3 (a) shows the impact of the base resistivity on the apparent $j_{0,met}$ as a function of F. The simulations are performed for a $n^+/n/n^+$ structure with $w = 40$ µm and $j_{0,met,sim} = 1000$ fA/cm². We see the same course of the curves with respect to F, as for Figure 2, where a description is given in Ref. [6]. For base resistivities of $\rho_B = 4.5$ Ωcm and $\rho_B = 2.5$ Ωcm the results are almost similar. By decreasing ρ_B further from $\rho_B = 2.5$ Ωcm to $\rho_B = 0.5$ Ωcm, the apparent $j_{0,met}$ decreases strongly resulting in values between $0.53 \lesssim j_{0,met}/j_{0,met,sim} \lesssim 0.70$. We assume, that the root cause for the behavior is the increased recombination current at the contact, which scales

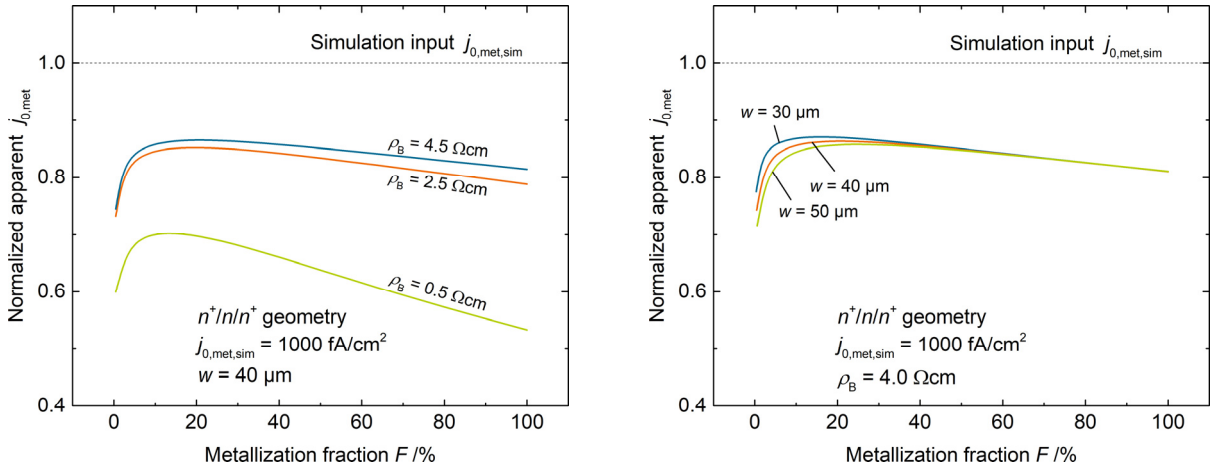

FIGURE 3: Apparent $j_{0,met}$ using the *area-weighted approach* normalized with the input of the simulation $j_{0,met,sim}$, given as a function of the metallization fraction F for a $n^+/n/n^+$ structure and $j_{0,met,sim}$ = 1000 fA/cm². (a) shows the impact of ρ_B for fixed w = 40 µm and (b) the impact of w, for fixed ρ_B = 4 Ωcm, on the resulting apparent $j_{0,met}$.

with the local *pn* product that increases due to the high doping level.

Figure 3 (b) shows the impact of the finger width w on the apparent $j_{0,met}$ as a function of F. The simulations are performed for a $n^+/n/n^+$ structure with ρ_B = 4.0 Ωcm and $j_{0,met,sim}$ = 1000 fA/cm². For F > 30% there is almost no difference between the different finger widths. For F < 30% wider fingers result in lower apparent $j_{0,met}$ values. As mentioned before, for high F values a vertical gradient in the *pn* product within the sample is dominant. For high metallization fractions F > 30%, this vertical gradient is almost independent of w and just depends on F and $j_{0,met,sim}$. Consistently, for F = 100%, (one side is fully metallized), the curves converge to the same value since here the gradient cannot depend on w. For small F values a lateral gradient of the *pn* product within the sample is dominant. By increasing w at constant F, the local *pn* product at the metal contact is pulled down more strongly, since the highly recombinative area is wider and therefore a larger quantity of charge carriers recombine in this very localized area (30 µm ≤ w ≤ 50 µm). As mentioned above, this results in a stronger underestimation of the *area-weighted approach*.

Experimental Comparison Between Area-Weighted and Simulative Approach

In this section, we show a comparison between the *area-weighted* and the *simulative approach* conducted for the metallized $n^+/n/n^+$ samples presented above. A similar analysis for one-sided laser ablated samples is found in Ref. [6].

Figure 4 shows the results of the evaluation. The blue squares indicate the average results using the measured QSSPC and PLI data as input for the *simulative approach*. For the metallization area fraction F we assume the finger width w = 40 µm similar to the screen opening, which might falsify the absolute value of $j_{0,met}$, but not the comparison between the two approaches. We see, that the average results for both F values are almost similar and result in a mean value of $j_{0,met}$ = (1528 ± 145) fA/cm².

The orange triangles indicate the average results using the same measured data as input for the *area-weighted approach*. For F = 4% this results in an apparent $j_{0,met}$ = (1213 ± 95) fA/cm² and for F = 13.3% in $j_{0,met}$ = (1285 ± 134) fA/cm². The error bars indicate the standard deviation σ of the respective results. Here, σ results from the analysis of two (F = 4%) or rather three (F = 13.3%) identically processed samples and is quite large in both cases indicating a large scattering of the results. We attribute this to the sample-to-sample variation of the identically processed samples.

The *area-weighted approach* underestimates $j_{0,met}$ by 16% to 20% compared to the *simulative approach*. Additionally, we see a slight upward trend in the apparent $j_{0,met}$ using the *area-weighted approach*, which is

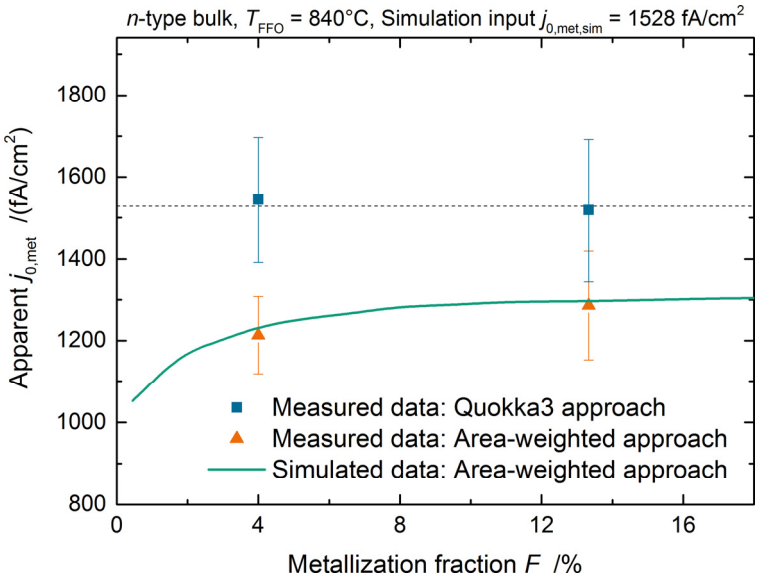

FIGURE 4: Apparent $j_{0,met}$ given as a function of F given for the metallized $n^+/n/n^+$ samples. The blue squares show the results applying the *simulative approach*, the orange triangles indicate the results applying *area-weighted approach* to the measured PLI and QSSPC data. Finally, the green line shows the results applying simulated data, generated by virtually replicating the metallized samples using the *area-weighted approach*.

expected due to the assumption of a uniform *pn* product, as discussed above. The green line in Figure 4 shows the results of the *area-weighted approach* applied to simulated data. To generate the simulated data, we replicate a sample—within a Quokka3 simulation—with the average characteristics (ρ_B, W,...) from the above evaluated metallized samples and set $j_{0,met,sim}$ = 1528 fA/cm² to the average value determined by the *simulative approach*. Thereafter, we simulate a QSSPC measurement and PLI measurements with varying metallization fractions F and evaluate the simulated data using the *area-weighted approach*. As expected, the simulated results are in good agreement with the measured data, confirming that the samples are replicated accurately, and similar physical models are used.

SUMMARY AND CONCLUSION

In the first part of this work, an *area-weighted approach* to determine the locally enhanced dark saturation current density at the metal contact $j_{0,met}$ is evaluated. It is already known that this approach delivers results, which underestimate $j_{0,met}$ due to the assumption of a uniform *pn* product within the sample. We find, that the degree of underestimation of the simple *area-weighted approach* for all metallization fractions F strongly depends on the actual $j_{0,met}$ itself and also on ρ_B for a base doping $\rho_B < 2.5$ Ωcm. For $F < 20\%$ the sample geometry where an emitter is present ($p^+/n/p^+$ structure) results in a noticeable weaker underestimation of $j_{0,met}$ compared to the geometry without emitter ($n^+/n/n^+$ structure). For almost all investigated parameters, the underestimation is at least 10%.

In the second part, the *area-weighted approach* is compared to a *simulative approach* based on numerical simulations using Quokka3. Therefore, one sided metallized samples with varying metallization fraction F are processed. For the data obtained from the metallized samples, the *area-weighted approach* leads to apparent $j_{0,met}$ values 16% to 20% lower than the $j_{0,met}$ results using the *simulative approach*.

The analysis in this work shows, that the *area-weighted approach* delivers results with varying accuracy, which strongly depend on the sample properties. We highly recommend using an evaluation method, which considers the non-uniformity of the *pn* product within the sample, either analytical or numerical. If not accessible, the sample properties should be chosen such that the underestimation is minimized, e.g high base resistivity and surfaces with *pn* junctions. The results obtained in this way, as well as literature data using the *area-weighted approach,* should be corrected—e.g. by extrapolating from this work (Figure 2 and Figure 3) if applicable.

ACKNOWLEDGMENTS

This work was supported by the German Federal Ministry for Economic Affairs and Energy BMWi and by the industry partners within the research project POLDI under contract No. 0324079D. The authors would like to thank Sebastian Meier-Meybrunn and Jonas D. Huyeng for support with simulations. David Herrmann would like to thank the "Deutsche Bundesstiftung Umwelt" for funding his dissertation project.

REFERENCES

1. S. Wasmer, A. A. Brand, J. M. Greulich, "Metamodelling of numerical device simulations to rapidly create efficiency optimization roadmaps of monocrystalline silicon PERC cells", Energy Procedia, 214C (2017).
2. B. Min, M. Muller, H. Wagner, G. Fischer, R. Brendel, P. P. Altermatt et al., "A Roadmap Toward 24% Efficient PERC Solar Cells in Industrial Mass Production", IEEE J. Photovoltaics, 7(6), 1541–1550 (2017).
3. J. Wong, S. Duttagupta, R. Stangl, B. Hoex and A. G. Aberle, "A Systematic Loss Analysis Method for Rear-Passivated Silicon Solar Cells", IEEE J. Photovoltaics, 5(2), 619–626 (2015).
4. A. Edler, V. D. Mihailetchi, L. J. Koduvelikulathu, C. Comparotto, R. Kopecek and R. Harney, "Metallization-induced recombination losses of bifacial silicon solar cells", Prog. Photovolt: Res. Appl., n/a (2014).
5. T. Fellmeth, A. Born, A. Kimmerle, F. Clement, D. Biro and R. Preu, "Recombination at metal-emitter interfaces of front contact technologies for highly efficient silicon solar cells", Energy Procedia, 8, 115–121 (2011).
6. D. Herrmann et al., "to be published".
7. R. Dumbrell, M. K. Juhl, T. Trupke and Z. Hameiri, "Extracting Metal Contact Recombination Parameters From Effective Lifetime Data", IEEE J. Photovoltaics, 1–8 (2018).
8. A. Fell, J. Schön, M. C. Schubert and S. W. Glunz, "The concept of skins for silicon solar cell modeling", Sol. Energy Mater. Sol. Cells, 173, 128–133 (2017).
9. M. Ernst, A. Fell, E. Franklin and K. J. Weber, "Characterization of Recombination Properties and Contact Resistivity of Laser-Processed Localized Contacts From Doped Silicon Nanoparticle Ink and Spin-On Dopants", IEEE J. Photovoltaics, 7(2), 471–478 (2017).
10. D. Herrmann, S. Lohmüller, H. Höffler, A. Fell, A. A. Brand and A. Wolf, "Challenges for the Quantification of Metal Induced Recombination Losses", 6 pages / 35th European Photovoltaic Solar Energy Conference and Exhibition; 287-292 (2018).
11. R. A. Sinton and A. Cuevas, "A quasi-steady-state open-circuit voltage method for solar cell characterization", 2000, pp. 1152–1155.
12. W. Götz, G. Pensl, W. Zulehner, R. C. Newman and S. A. McQuaid, "Thermal donor formation and annihilation at temperatures above 500 °C in Czochralski-grown Si", J. Appl. Phys., 84(7), 3561–3568 (1998).
13. S. Werner, E. Lohmüller, P. Saint-Cast, J. M. Greulich, J. Weber, S. Maier et al., "Key aspects for fabrication of p-type Cz-Si PERC solar cells exceeding 22% conversion efficiency", 2017.
14. A. Kimmerle, J. Greulich and A. Wolf, "Carrier-diffusion corrected J0-analysis of charge carrier lifetime measurements for increased consistency", Sol. Energy Mater. Sol. Cells, 142, 116–122 (2015).